sciendo

POLISH MARITIME RESEARCH 3 (123) 2024 Vol. 31; pp. 4-14
10.2478/pomr-2024-0031

Numerical Study on the Effect of Weight Variables on the Roll Damping Coefficients for a Fishing Vessel

Janghoon Seo [1]
Dong-Woo Park [2*]
[1] Shipbuilding & Marine Simulation Center, Tongmyong University, Busan, Republic of Korea
[2] Department of Marine Mobility, Tongmyong University, Busan, Republic of Korea

* Corresponding author: *dwpark@tu.ac.kr (Dong-Woo Park)*

ABSTRACT

The roll damping coefficient is essential when considering the viscous effect in the potential-based hydrodynamic analysis of fishing vessels; it is an important factor in the roll motion response. The present study performs free roll decay simulations, altering weight variables using Computational Fluid Dynamics (CFD) to investigate the correlation between the roll damping coefficient and the weight variation of a fishing vessel. The time series of roll amplitude and roll damping coefficient are compared, for varying vertical and longitudinal centres of gravity and radii of gyration in roll motion. As the vertical centre of gravity increases, both the roll decay period and the roll damping coefficient also increase. The roll decay period tends to increase with the increase in the radius of gyration during roll motion, while the roll damping coefficient exhibits a decrease. A longitudinal centre of gravity has a limited effect on free roll decay characteristics. The roll damping coefficients between the maximum and minimum combinations of weight variables show significant differences. The findings of the present study could enhance the understanding of the safety of fishing vessels based on their loading conditions. Consequently, future research could further improve the results obtained in the present study by considering various hull shapes and speeds.

Keywords: Free roll decay, Roll damping coefficient, Fishing vessel, Computational fluid dynamics, Weight variable

INTRODUCTION

Ship motion is one of the critical factors affecting the safety and stability of ships and offshore structures. In particular, ship motion is more important for small vessels than for large vessels because small vessels exhibit a larger motion response to environmental loads. A ship's motion is typically estimated using potential-based approaches or experiments. However, potential-based approaches do not account for governing viscous effects, which are essential when considering roll motion. Thus, an additional damping coefficient is required as an input to the potential-based approach, to address viscous effects.

In general, empirical methods are used to estimate viscous roll damping coefficients. The most widely employed approach is the empirical method proposed by Ikeda et al. [1], in which the equivalent total damping coefficient is determined by summing the contributions of friction, eddy-making, and wave-making components. Ikeda's extended roll damping study considered the effect of appendages and forward speed on roll damping [2-5]. Chakrabarti [6] also proposed a method for estimating roll damping for ships and barges using an empirical method.

Roll damping estimations for naval ships (and ships in general) were conducted in previous research, either through experiments or by using Computational Fluid Dynamics (CFD).

Previous research investigated methods for calculating the roll damping coefficient using free roll decay motion [7-12] or harmonic-excited roll motion [13-16]. The studies were performed by considering the interaction between bilge keels and other structures [17-20].

In addition to the previous research on general and naval ships, roll damping studies for small vessels have mainly been conducted through experiments. Haddara and Bass [21] studied the characteristics of roll damping coefficients for three different (small) fishing vessels, and Chun et al. [22] confirmed the effect of the bilge keel and central wing on the roll damping characteristics of a small fishing vessel. Ali et al. [23] investigated the roll damping characteristics of a fishing boat with and without drift motion and highlighted the over estimation of roll response in heavy seas. Ayob and Yaakob [24] performed free roll decay simulations of the effects of devices used to reduce roll motion in small fishing boats. Hasanudin et al. [25] confirmed the influence of bilge keels on roll motion in fishing boats and Katayama et al. [26] derived roll damping coefficients for planning hulls. Recently, Zhang et al. [27] performed experiments and CFD for roll damping estimations with various hull forms of a trimaran vessel; they compared the results of free roll decay curves between the results of the experiments and CFD.

Most of the previous research on the roll damping coefficient of small vessels focused on estimation methods and the effect of appendages. To the best of our knowledge, there has only been limited research into estimating the effect of weight location and distribution on roll damping coefficients for small vessels. Zhou et al. [28] derived roll damping coefficients for four different types of ships by the CFD approach. They investigated the effect of the Vertical Centre of Gravity (VCG) of the container vessel on the roll damping coefficient but did not consider the small vessel and the variation of radius of gyration in roll motion (Kxx). Hasanudin et al. [29] used Kxx for the sensitivity analysis of the Generalized Reduced Gradient (GRG) method, to optimise free roll decay results. However, they did not figure out the effect of Kxx.

Moreover, the distribution and location of weight may differ from the design criteria due to the situation and environment of the work. These deviations may result in overloading or improper loading of the weight on a fishing vessel, leading to significant problems and serious accidents [30-32]. Therefore, a study of roll motion characteristics, by changing the weight of a fishing vessel, is required.

In the present study, we investigate the roll damping characteristics of a small fishing vessel by altering weight variables. Free roll decay simulations are conducted using CFD with altered weight locations and distributions, and the differences in roll damping coefficients are assessed. Based on the results, our aim is to identify and compare the weight variables that have the most significant influence on the roll damping coefficient. In addition, the change in metacentre, a critical factor for the safety of fishing vessels, is investigated, based on the results obtained from the free roll decay simulation.

FISHING VESSEL AND CONDITIONS

In the present study, a 4.99 ton Korean standard fishing vessel was employed. The shape of this fishing vessel is presented in Fig. 1. A box keel was attached to the baseline and other appendages were not considered. The main particular loading conditions of the fishing vessel are presented in Table 1. The speed of the vessel was set to zero. The initial radius of gyration in roll motion was assumed to be 0.35B. The added mass moment of inertia in the roll axis was derived at the natural period of roll motion.

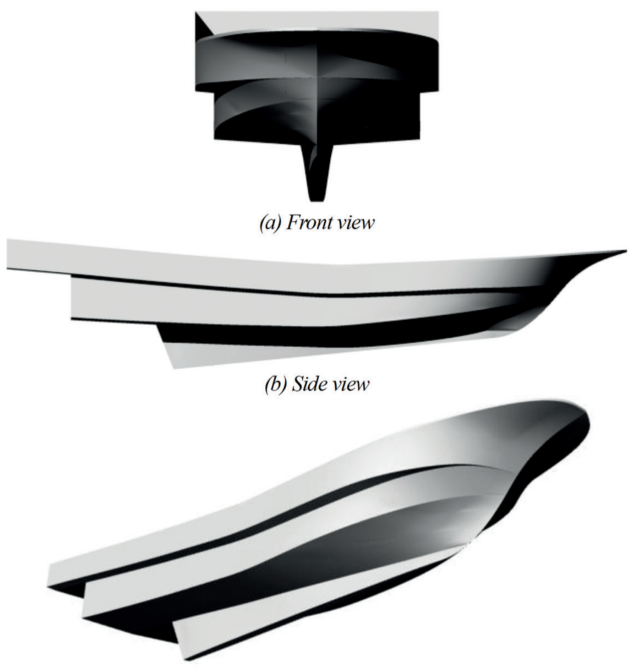

Fig. 1. Hull shapes of fishing vessel

Tab. 1. Main particulars and loading conditions of fishing vessel

Description	Symbol	Value	Units
Length between perpendicular	L_{BP}	11.2	m
Breadth	B	3.3	m
Depth	D	1.55	m
Displacement	Δ	20.8	ton
Draft at midship	d	0.69	m
Longitudinal centre of gravity from after perpendicular	LCG	4.664	m
Vertical centre of gravity from baseline	VCG	1.323	m
Radius of gyration in roll motion	Kxx	1.155	m
Metacentric height in transverse direction	GM_T	0.440	m
Hydrostatic stiffness of heave motion	C33	342993.16	N/m
Hydrostatic stiffness of roll motion	C44	927.581	N·m/°
Hydrostatic stiffness of pitch motion	C55	50897.063	N·m/°
Added mass moment of inertia in roll axis	A44	6.937	ton·m²

Tab. 2. Analysed cases by weight variables of the fishing vessel

VCG		Kxx		LCG	
Case	Value (×VCG)	Case	Value	Case	Value (×LCG)
VCG1	0.90	Kxx1	0.25	LCG1	0.90
VCG2	0.95	Kxx2	0.30	LCG2	0.95
VCG3	1.00	Kxx3	0.35	LCG3	1.00
VCG4	1.05	Kxx4	0.40	LCG4	1.05
VCG5	1.10	Kxx5	0.45	LCG5	1.10

In order to investigate the effects of weight location and distribution, various weight positions along the longitudinal and vertical directions were considered. The VCG was adjusted by ±5% and ±10% from the original VCG, and the LCG was varied by ±5% and ±10% from the original LCG. Simultaneously, the trim change of the fishing vessel, due to the LCG change, was taken into account. The Kxx was varied from 0.25B to 0.45B at intervals of 0.05B. The analysed cases for the VCG, Kxx, and LCG variations were defined as VCG1 to VCG5, Kxx1 to Kxx5, and LCG1 to LCG5, respectively, as shown in Table 2.

NUMERICAL APPROACH

GOVERNING EQUATIONS

The governing equations for unsteady incompressible viscous flow are the continuity and Navier-Stokes equations used to solve the free roll decay of the fishing vessel. These equations can be presented in a Cartesian tensor form as:

$$\frac{\partial(\rho\bar{u}_l)}{\partial t} = 0 \quad \textbf{(1)}$$

$$\frac{\partial}{\partial t}(\rho\bar{u}_l) + \frac{\partial}{\partial x_j}(\rho\bar{u}_l\bar{u}_J) = -\frac{\partial\bar{p}}{\partial x_i} + \frac{\partial}{\partial x_j}\left[\mu\left(\frac{\partial\rho\bar{u}_l}{\partial x_j} + \frac{\partial\rho\bar{u}_J}{\partial x_i}\right)\right] + \frac{\partial}{\partial x_j}\left(-\overline{\rho u_l' u_J'}\right) + \rho g_i \quad \textbf{(2)}$$

where x_i are the Cartesian coordinates, $\bar{u}_l$ are the corresponding velocity components, t is the time and $\bar{p}$, ρ, μ and g are the pressure, density, viscosity and gravity, respectively.

A Reynolds stress term of $-\overline{\rho u_l' u_J'}$ was derived by employing the realisable k–ε turbulence model, which was applied in previous studies [10, 12, 15]. k is the kinetic energy per unit mass and is the turbulent dissipation, making it suiTable for interactions between external incompressible flow and complex geometry. The transport equations of the realisable k–ε turbulence model for k and ε can be written as:

$$\frac{\partial}{\partial t}(\rho k) + \frac{\partial}{\partial x_j}(\rho k u_j) = \frac{\partial}{\partial x_j}\left[\left(\mu + \frac{\mu}{\sigma_k}\right)\frac{\partial k}{\partial x_j}\right] + G_k + G_b - \rho\epsilon - Y_M + S_k \quad \textbf{(3)}$$

$$\frac{\partial}{\partial t}(\rho\epsilon) + \frac{\partial}{\partial x_j}(\rho\epsilon u_j) = \frac{\partial}{\partial x_j}\left[\left(\mu + \frac{\mu_t}{\sigma_\epsilon}\right)\frac{\partial\epsilon}{\partial x_j}\right] + \rho C_1 S_\epsilon - \rho C_2\frac{\epsilon^2}{k+\sqrt{\nu\epsilon}} - C_{1\epsilon}\frac{\epsilon}{k}C_{3\epsilon}G_b + S_\epsilon \quad \textbf{(4)}$$

where $C_1 = \max[0.43, \eta/(\eta{+}5)$, $\eta = S(k/\epsilon)$, $S = \sqrt{2S_{ij}S_{ij}}$ and G_k represents the generation of turbulence kinetic energy due to the mean velocity gradients, calculated in the same manner as the standard k–ε turbulence model.

The pressure-velocity coupling and the overall solution procedure were based on the semi-implicit method for the pressure-linked equation-consistent (SIMPLEC) algorithm. The SIMPLEC second-order scheme was used for pressure and convection terms, while a second-order central difference scheme was applied to diffusion terms. The volume of fluid (VOF) method was employed to simulate free-surface flow. To realise fishing vessel motions, the dynamic fluid body interaction (DFBI) method was applied. Analysis was performed using Star CCM+ software.

ROLL DAMPING ESTIMATION METHOD

The free roll decay simulation was performed to derive the roll damping coefficient of the fishing vessel. The equation of motion for the free roll decay simulation can be expressed as:

$$I\ddot{\phi} + B\dot{\phi} + C\phi = 0 \quad \textbf{(5)}$$

where I, B and C are the mass and added moment of inertia, damping coefficient and restoring coefficient of roll motion, respectively. $\ddot{\phi}$, $\dot{\phi}$ and ϕ are the acceleration, velocity and angle of roll motion, respectively.

Considering the non-linear viscous effect in the free roll decay simulation, the equation can be written as follows:

$$I\ddot{\phi} + B_l\dot{\phi} + B_q\dot{\phi}|\dot{\phi}| + C\phi = 0 \quad \textbf{(6)}$$

where B_l and B_q are the linear and quadratic damping, respectively.

The free roll decay simulation was performed as shown in Fig. 2. The simulation was initiated with a forced initial heeling angle of the fishing vessel and then the fishing vessel was released at the designated time. The roll motion subsequently decays due to fluid forces until the fishing vessel reaches an equilibrium state. The roll damping coefficient was determined using the relative decrement method, utilising the peak values from the time history of the roll angle [18]. The extinction curve could be fitted using the mean amplitude A_i and the decrement of the amplitude divided by the mean amplitude difference D_i of roll amplitudes, as shown in Fig. 3.

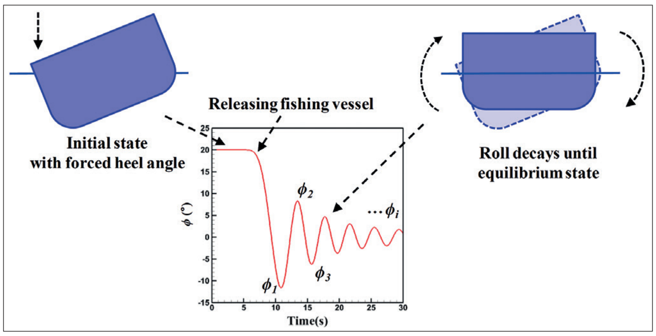

Fig. 2. Schematic of free roll decay simulation

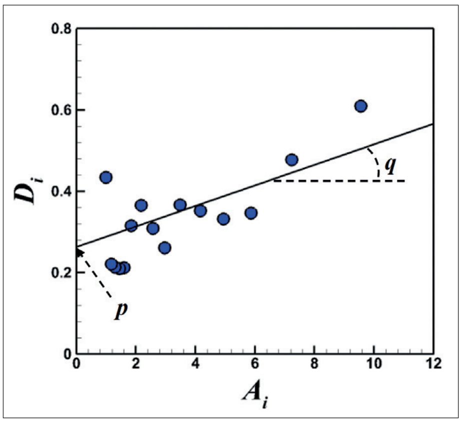

Fig. 3. Example of decay decrement analysis

$$D_i = p + qA_i \tag{7}$$

$$A_i = 0.5(|\phi_i| + |\phi_{i+1}|) \tag{8}$$

$$D_i = \left(0.5(|\phi_i| - |\phi_{i+1}|)/0.5(|\phi_i| + |\phi_{i+1}|)\right) \tag{9}$$

The linear and quadratic roll damping coefficients were obtained by the coefficients p and q that fit the decrement data points through the least-square method.

$$B_l = \frac{p}{\pi}\frac{C}{\omega_n} = 2p\frac{I}{T_d} \tag{10}$$

$$B_q = \frac{3}{8}q\frac{C}{\omega_n^{\ 2}} = \frac{3}{8}qI \tag{11}$$

where T_d is the decay period.

The equivalent linear damping can be written as:

$$B_e = B_l + B_q\frac{16}{3}\frac{\phi_a}{T_d} = 2(p + q\phi_a)\frac{I}{T_d} \tag{12}$$

where ϕ_a is the amplitude of roll motion.

The equivalent linear damping coefficient can be non-dimensionalised by the critical damping coefficient ($B_c = 2\sqrt{IC}$).

$$\zeta_R = \frac{B_e}{B_c} = \frac{1}{2\pi}(p + q\phi_a) \tag{13}$$

COMPUTATIONAL DOMAIN AND BOUNDARY CONDITIONS

The computational domain and boundary conditions are presented in Fig. 4. The overset mesh technique was applied to realise free roll decay motion of the fishing vessel. Thus, the cylindrical part (including the fishing vessel and the rectangular part of the overall computational domain) were set as rotating and stationary parts, respectively. The symmetry boundaries were located at the bottom, top and side faces of the computational domain. Velocity inlet and pressure outlet boundary conditions were considered for inflow and outflow boundaries, respectively. No-slip boundary conditions were defined on the surfaces of the fishing vessel.

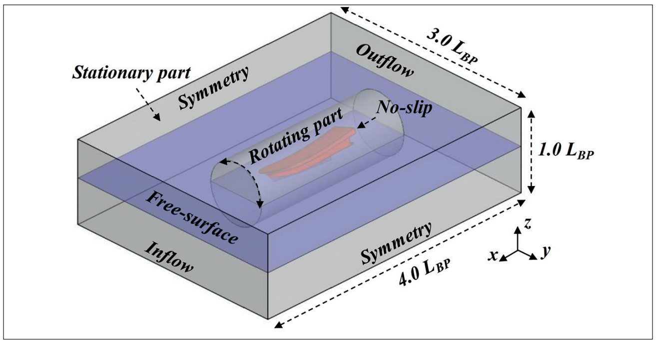

Fig. 4. Computational domain and boundary conditions

The computational domain was structured with dimensions of 4L, 3L, and 1L along the length, breadth, and height directions of the fishing vessel, respectively. These dimensions were based on previous research [8] and adjusted to account for the difference in ship speed by positioning the fishing vessel at the centre of the computational domain and increasing the size of the computational domain in the width direction of the ship.

GRID SYSTEM AND VALIDATION

The grid distribution applied in the present study is presented in Fig. 5. The Cartesian cut-cell method, with a prism mesh layer near the wall of the fishing vessel, was applied to improve the accuracy of the simulation. This arrangement consisted of six prism layers with an expansion ratio of 1.3. The minimum grid spacing near the fishing vessel, with a wall y+ value close to 5, was approximately 0.003 m. Grids were concentrated near the rotating part and free-surface, and the mesh size was gradually increased as it moved to the outer boundary.

A grid dependency test was conducted using three different grid configurations to assess the impact of grid systems on free roll decay calculations. Three different systems; coarse, medium and fine grids, with 2.0, 4.5, and 6.0 million grids, were applied, respectively. The grid distributions of the three systems are compared in Fig. 6. To verify the differences between grid systems, the time series of roll angle during free roll decay calculations were compared. The results of the grid dependency test showed that the difference in time series of the roll angle is negligible between the medium and fine grid system, as shown in Fig. 7. Therefore, the medium grid system was employed in further studies.

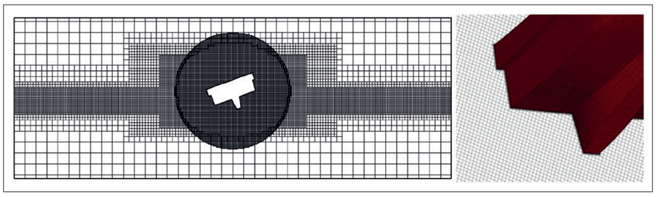

Fig. 5. Grid distributions

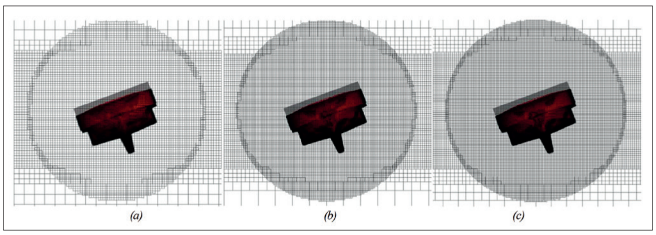

Fig. 6. Grid distributions of (a) Coarse, (b) Medium and (c) Fine grid system

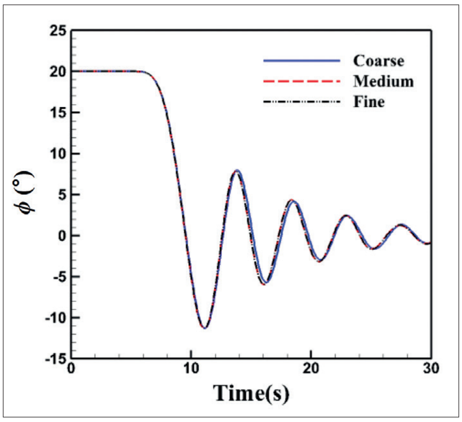

Fig. 7. Results of grid dependency test

To validate the numerical configurations, a comparison of roll damping coefficient for a box type barge was conducted. The shape of the box type barge applied was defined in previous research [33] and is presented in Fig. 8. The averaged decay time, linear and quadratic damping coefficients were compared with the experimental results. The present results give good agreement with the experimental results, as shown in Table 3. Therefore, the numerical conditions and grid system employed in the present study are suiTable for the free roll decay simulation.

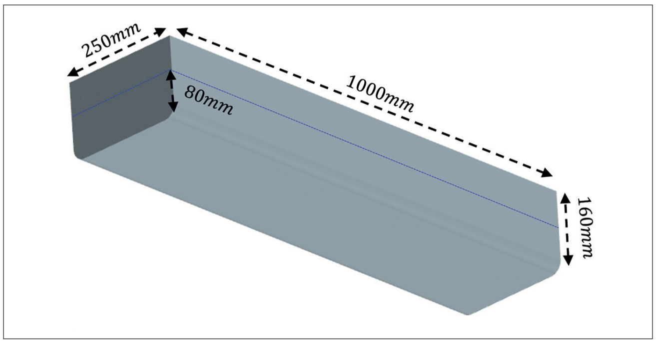

Fig. 8. Hull shape of the barge model for validation

Tab. 3 Validation for the barge model with previous data

Item	Present	Kim et al. [33]	Absolute difference
T_d	1.2	1.2	0.0
p	0.0527	0.0531	0.0040
q	0.0065	0.0019	0.0046
ζ_R	0.839	0.845	0.006

RESULTS AND DISCUSSION

EFFECT OF VCG VARIATION

First of all, the results of the free roll decay simulation were investigated according to the variation of VCG. The analysed cases from VCG1 to VCG5 (as defined in Table 2) were employed and the results of the time histories of roll angle are presented in Fig. 9. After the free roll decay commenced, the 1st and 2nd peaks showed no significant differences in the roll period and amplitude. It was subsequently confirmed that the free roll decay period increases with an increasing VCG. The increase in VCG is associated with the decrease of metacentre, leading to an increase in period, which is related to the generally known 'natural roll period' of the vessel ($\omega_n = \sqrt{\Delta g GM_T / I}$).

The difference in roll amplitude, along with the change in decay period, becomes more remarkable as the decay simulation progresses. The roll amplitude decreases with increasing VCG and this becomes clear after a specific time. The difference in roll amplitude between VCG1 and VCG5 becomes approximately two times greater after the 7th peak. The decrease in roll amplitude can be attributed to the variation in the roll moment arm with the increase in VCG.

In order to quantitatively assess the difference in roll damping with VCG change, the roll damping coefficients are derived using the time histories of free roll decay simulation. The roll damping coefficient and damping period obtained from the time histories of free roll decay simulation are shown in Fig. 10. The horizontal axis represents the VCG cases, the left vertical axis represents the damping coefficient, and the right vertical axis represents the amplitude of the period. In addition, the linear and quadratic components of non-dimensionalised roll damping coefficient are also presented.

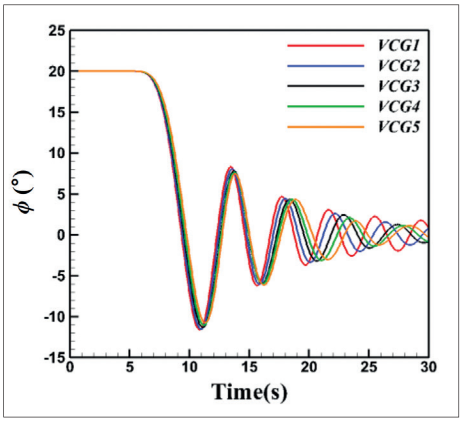

Fig. 9. Comparison of time histories of roll amplitude with different VCGs

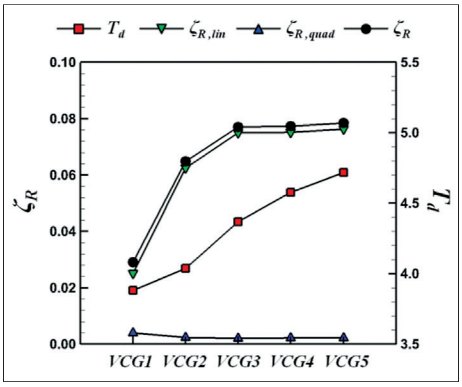

Fig. 10. Comparison of relative roll damping coefficients with different VCGs

Fig. 11. Instantaneous contours of vorticities and velocity vector fields at the 1st peak in the longitudinal plane () of (left column) and (right column)

The roll decay period increases with an increasing VCG, as shown in Fig. 9. The linear damping coefficient increases with an increasing VCG but the rate of increase slows down with higher VCG. Quadratic damping shows a tendency to decrease with

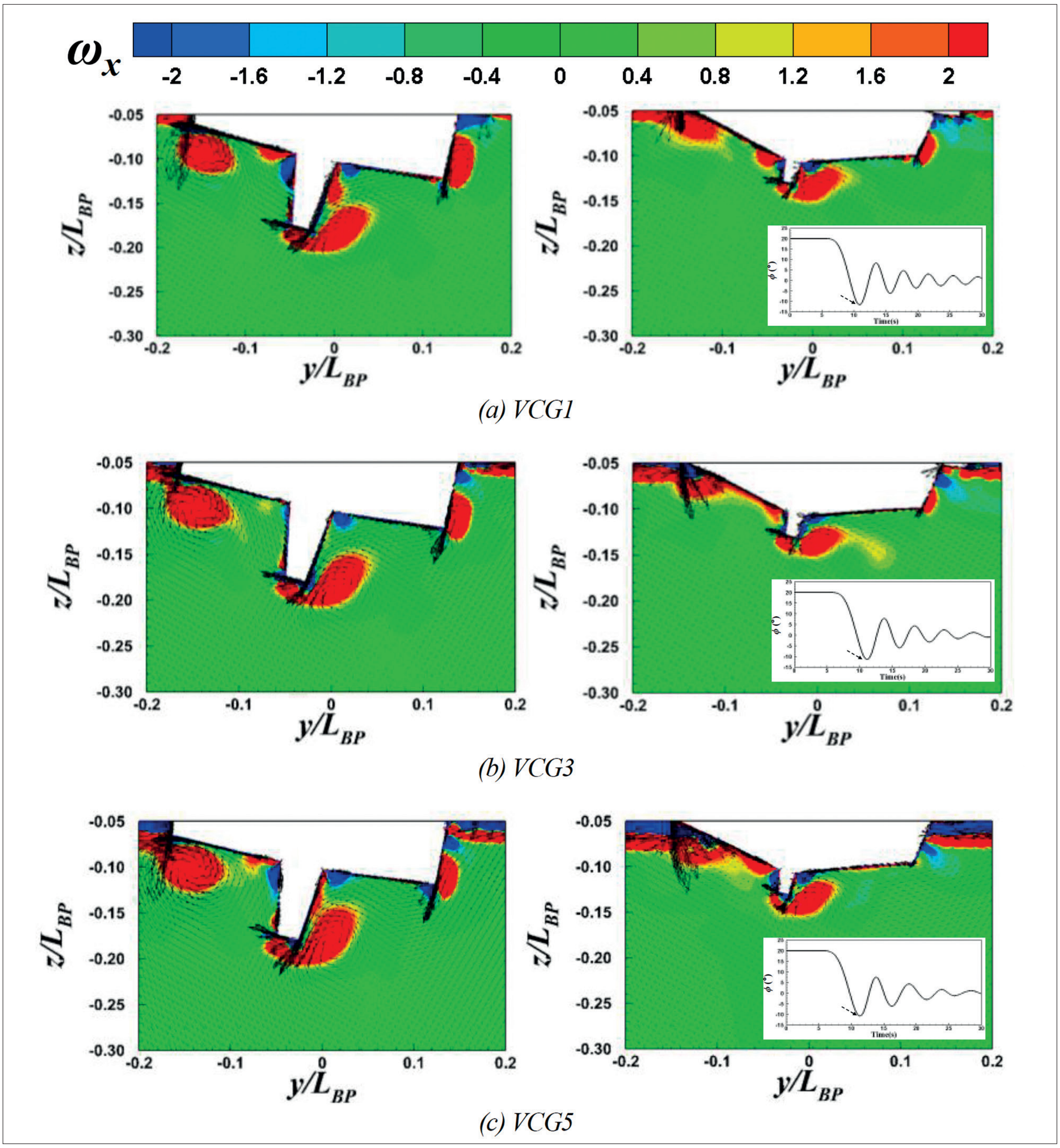

Fig. 11. Instantaneous contours of vorticities and velocity vector fields at the 1st peak in the longitudinal plane (y–z) of x=0.25L$_{BP}$ (left column) and x=0.75L$_{BP}$ (right column)

an increasing VCG but the amplitude of quadratic damping is not significant. As a result, the tendency of the equivalent linear damping is similar to that of the linear damping coefficient.

To investigate the correlation between the damping coefficient and period of free-roll decay simulation and flow characteristics, the flow field around a fishing vessel was examined. The contours of stream-wise vorticity and velocity vectors in the *y-z* plane at the 1st peak are shown in Fig. 11. VCG1, VCG3, and VCG5 were selected as representative cases.

When a fishing vessel is in the 1st peak, the vessel is in the maximum negative rotational direction, which leads to the generation of positive vorticity in the opposite direction to the fishing vessel's rotation. Large vortices are generated at the corners and box keel of fishing vessels. In the plane close to the bow, the shape of the box keel is reduced and the corner angle increases. This leads to a decrease in the vorticity around the box keel. It can be confirmed that the overall difference in the flow field is not significant because the roll amplitude and period are not markedly different at the 1st peak, as shown in Fig. 9.

In contrast, the differences in flow characteristics relating to the variations in VCG become apparent after several time periods. The instantaneous flow fields at the 6th peak under each VCG condition are shown in Fig. 12. At the 6th peak, the vessel is in the maximum positive rotational direction and negative vorticity is located around the fishing vessel. The magnitude and distribution of vorticity at the 6th peak are smaller than

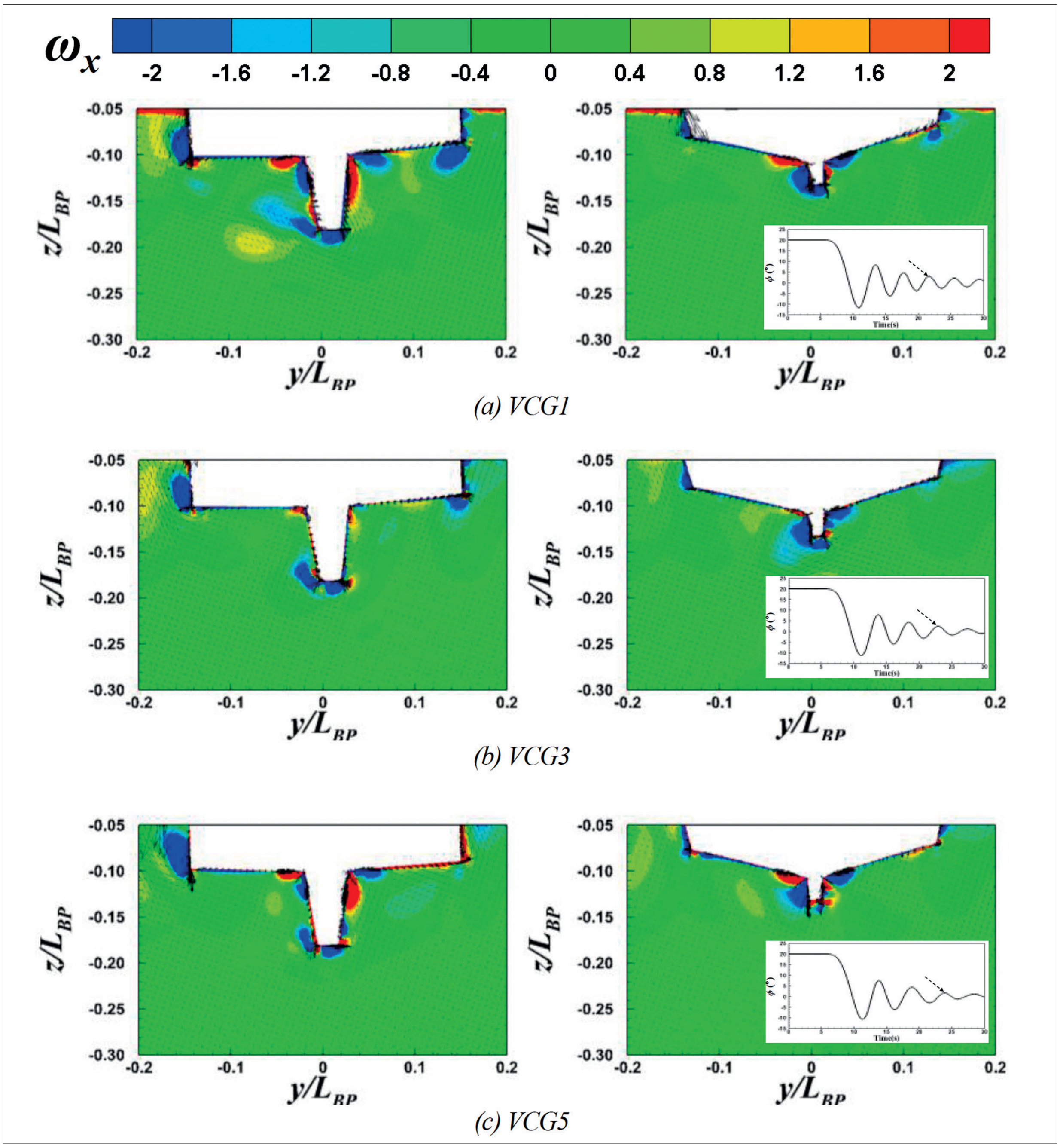

Fig. 12. Instantaneous contours of vorticities and velocity vector fields at the 6th peak in the longitudinal plane (y–z) of x=0.25L_{BP} (left column) and x=0.75L_{BP} (right column)

that of the 1st peak. This is because the roll motion is reduced as free-decay progresses sufficiently, resulting in smaller vortices forming around the vessel.

In the case of VCG1, the decay of roll motion is relatively insufficient compared to other VCG conditions at the 6th peak (Fig. 12(a)). As a result, it has a relatively large wake structure around the fishing vessel. On the other hand, the size of the wake structure on the portside of the fishing vessel in the case of VCG3 is smaller than that of the case of VCG1 (Fig. 12(b)). Finally, the wake structure generated on the portside disappears in the case of VCG5 (Fig. 12(c)). This is because a large wake structure does not develop but is sufficiently dissipated due to the increased decay period when the VCG is high at the same peak, as shown in Fig. 9. Consequently, the flow field around a fishing vessel under different VCG is related to the change in decay period.

EFFECT OF KXX VARIATION

The time series of roll amplitude, as a result of the free roll decay simulation with Kxx variation, is shown in Fig. 13. Differences in roll amplitude are observed after the initial peak. As Kxx increases, the roll peak also increases and this tendency does not change, even after the decay has sufficiently progressed. The roll period is shown to follow the same tendency as Kxx. The increase in Kxx implies that the vessel's natural period also increases. This correlation, between roll amplitude and Kxx, can be attributed to the relationship whereby a larger Kxx corresponds to an increase in angular momentum.

The free roll decay period and damping coefficients, as a function of Kxx, are shown in Fig. 14. As shown in Fig. 13, the decay period increases linearly with increasing Kxx. On the other hand, the roll damping coefficient is decreased as Kxx increases. This is attributed to the large angular momentum, despite the increase in period. Similar to VCG variation, the quadratic damping coefficient is smaller than the linear damping coefficient. As a result, the non-dimensionalised roll damping coefficient follows the tendency of the linear damping coefficient.

The stream-wise vorticity distributions on multiple y-z planes around the hull are depicted in Fig. 15. The analysed cases of Kxx1, Kxx3, and Kxx5 at the 1st and 2nd peaks are selected as being representative. Both peak periods have relatively larger magnitudes of vorticity at Kxx1, where Kxx is the smallest condition.

Kxx5 has a large roll amplitude, as shown in Fig. 13, but the magnitude of the vorticity structure is not high due to the relatively long period. For Kxx1, which has a relatively short period, the vorticity magnitude is relatively high.

EFFECT OF LCG VARIATION

Fig. 16 shows the time histories of roll amplitude with different LCGs. In contrast to the results of free roll decay for variations in VCG and Kxx, the effect of LCG is limited. As the decay progresses, the effect of LCG is subtly observed. The roll period increases as LCG decreases. In the case of roll amplitude, the difference due to the variation in LCG is also minor. These changes are identified in the damping coefficient and roll period shown in Fig. 17. In the case of roll damping coefficient, there is a small increase with LCG increase but it is significantly smaller than the difference due to variations in VCG and Kxx. As a result, the change in LCG does not have a significant impact on the free roll decay characteristics.

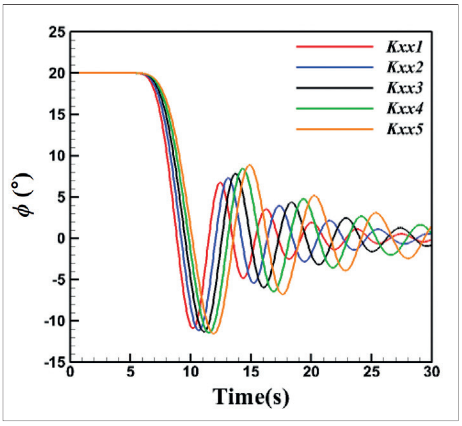

Fig. 13. Comparison of time histories of roll amplitude with different Kxx

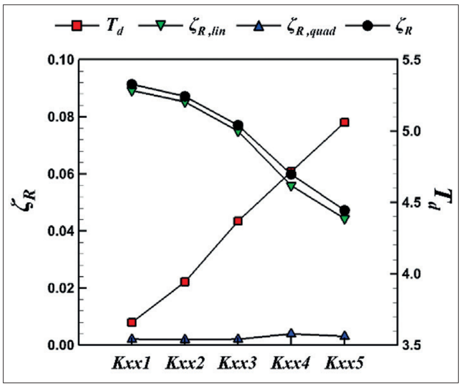

Fig. 14. Comparison of relative roll damping coefficients with different Kxx

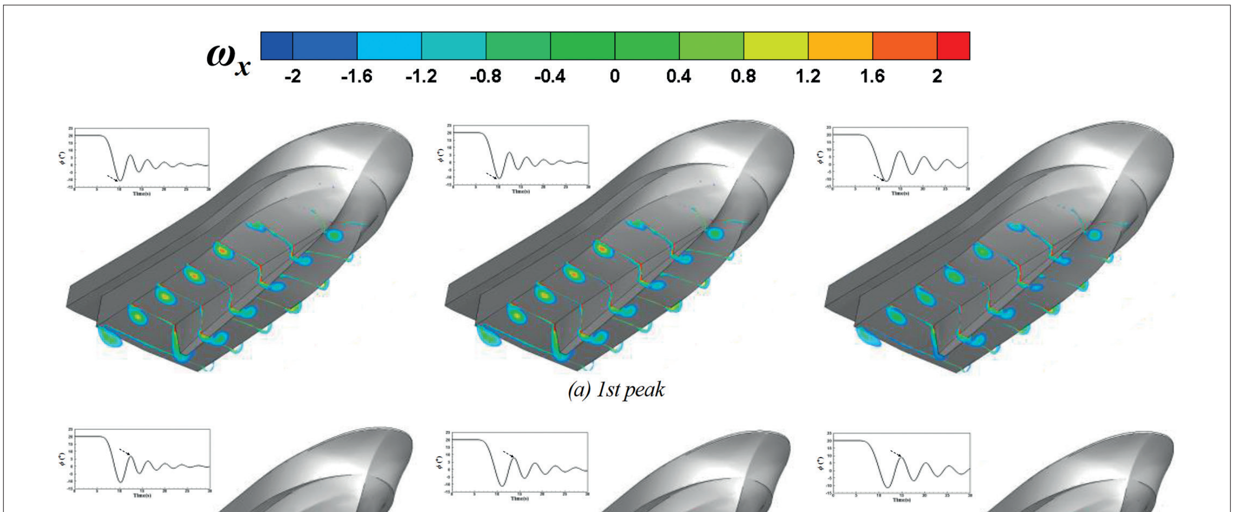

Fig. 15. Contours of vorticities and velocity vector fields of Kxx1 (left column), Kxx3 (middle column), and Kxx3 (right column)

COMPARISON BETWEEN THE MAXIMUM AND MINIMUM COMBINATION OF WEIGHT VARIABLES

Based on the results of the free roll decay simulations for different values of VCG, Kxx, and LCG, additional free roll decay simulations were performed for the combinations of variables that have the greatest and smallest effects on the damping coefficient. The combination of VCG1 and Kxx5 (VCG1-Kxx5) was selected as the case with the smallest roll damping coefficient, while the combination of VCG5 and Kxx1 (VCG5-Kxx1) was selected as the case with the largest roll damping coefficient. LCG variation was excluded due to the limited effect of LCG. The results of the free roll decay for the two combinations are shown in Fig. 18. The results show that the roll amplitude of the combination with the largest roll damping coefficient (VCG5-Kxx1) decays relatively quickly, while the roll amplitude of the combination with the smallest roll damping coefficient (VCG1-Kxx5) decays relatively slowly. In the case of a non-dimensionalised roll damping coefficient, VCG5-Kxx1 and VCG1-Kxx5 showed 0.125 and 0.0318, respectively, and the periods showed differences of 0.581 s and 0.685 s. The maximum difference of roll damping coefficient between the two cases is about 10%.

INFLUENCE OF DYNAMIC EFFECTS ON GM

Typically, the GM_T in a calm sea is derived from hydrostatic values, including the vertical centre of buoyancy (VCB), displacement, the second moment of inertia of the water plane area, and the VCG. However, the GM_T value can also be affected by dynamic effects, due to the roll motion of the vessel. Thus, GM_T in a calm sea obtained from hydrostatic values and denoted as GM_T_C, is compared with that estimated using the roll natural period from the decay simulation (GM_T_E), as shown in Fig. 19. The difference between GM_T_C and GM_T_E shows an increasing tendency as the VCG increases (Fig. 19(a)). This can be attributed to the dynamic behaviour of the fishing vessel as VCG increases, leading to an increase in the period (Fig. 10). Changes in Kxx do not directly affect the GM_T_C but the resulting changes in Td indirectly influence GM_T_E, as shown in Fig. 19(b). As Kxx increases or decreases, T_d also changes (Fig. 14), leading to a gradual increase in the difference compared to the GM_T_C.

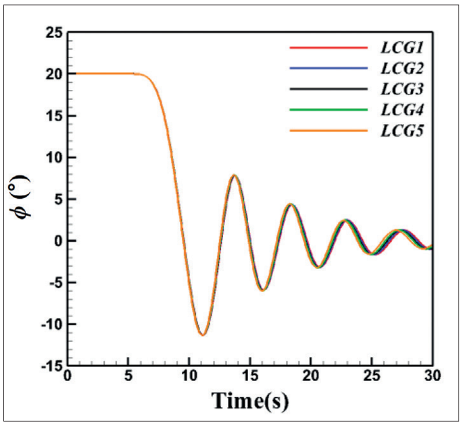

Fig. 16. Comparison of time histories of roll amplitude with different LCGs

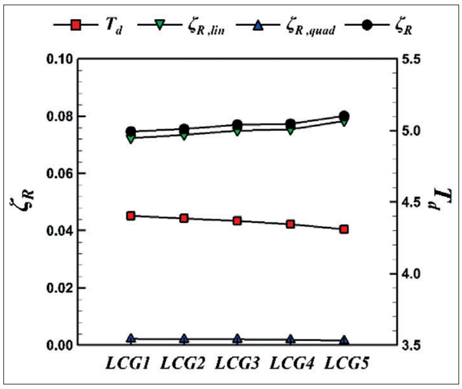

Fig. 17. Comparison of relative roll damping coefficients with different LCGs

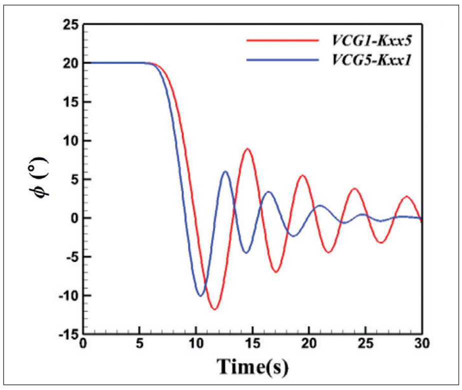

Fig. 18. Comparison of time histories between maximum and minimum combinations of weight variables

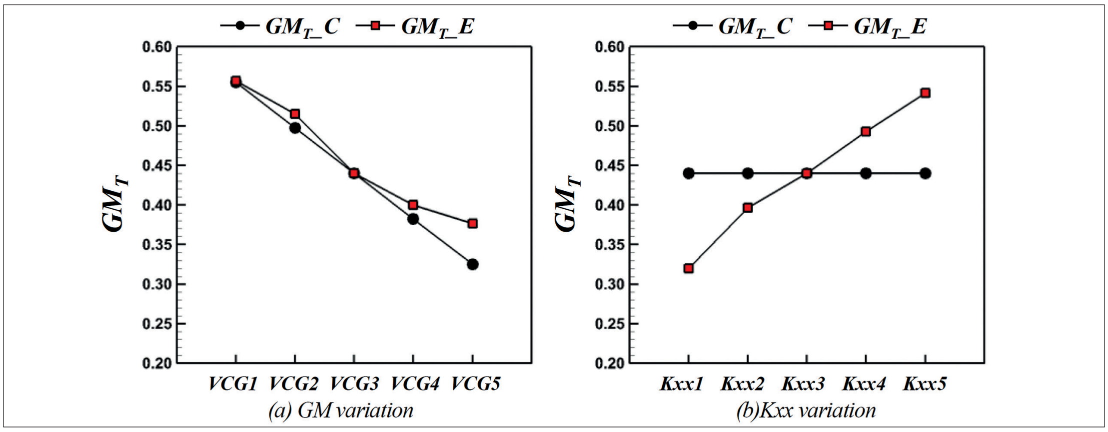

Fig. 19. Comparison of GMT by typical calculation and derived from TD with variable parameters

CONCLUSIONS

In the present study, the characteristics of free roll decay are assessed for fishing vessels with different weight variables. Free roll decay simulation is performed by CFD calculation, considering weight variables of the vertical and longitudinal centre of gravity and radius of gyration in roll motion. Time series of roll amplitude and roll damping coefficient are compared to assess the effect of weight variables. As the vertical centre of gravity increases, the roll decay period and roll damping coefficient increase. The roll decay period increases as the radius of gyration in roll motion increases but the roll damping coefficient decreases. The effect of the longitudinal centre of gravity is limited to the period and damping coefficient of roll decay. The difference in roll damping coefficients between the maximum and the minimum combinations of weight variable is about 10%. Additionally, the difference between the estimated GM obtained from the roll damping period and the GM derived from hydrostatic values is compared. The results of this study may provide information on the changes in the safety of fishing vessels depending on the loading condition. Therefore, the additional assessment of the characteristics of free roll decay with various hull shapes and speeds should be supplemented through future research.

ACKNOWLEDGEMENTS

This work was supported by the establishment of software predicting roll motion and safety of fishing vessel based on D.N.A. grant funded by the KOrea Maritime transportation Safety Authority(KOMSA).

REFERENCES

1. Ikeda Y, Himeno Y, Tanaka N. On eddy making component of roll damping force on naked hull, Journal of the Society of Naval Architects of Japan, 1977. https://doi.org/10.2534/jjasnaoe1968.1977.142_54.

2. Ikeda Y, Himeno Y, Tanaka N. Components of roll damping of ship at forward speed, Journal of the Society of Naval Architects of Japan, 1978a. https://doi.org/10.2534/jjasnaoe1968.1978.113.

3. Ikeda Y. On roll damping force of ship-effect of friction of hull and normal force of bilge keels, University of Osaka Prefecture, Department of Naval Architecture, Japan, Report No. 00401, Published in: Journal of Society of Naval Architects of Japan, 1978b.

4. Ikeda Y, Umeda N. A prediction method of roll damping of a hardchine boat at zero forward speed, Journal of the Kansai Society of Naval Architects, 1990, p. 213.

5. Ikeda Y, Fujiwara T, Katayama T. Roll damping of a sharp cornered barge and roll control by a new-type stabilizer. In: Proc. 3rd International Society of Offshore and Polar Engineers Conference, 1993.

6. Chakrabarti S. Empirical calculation of roll damping for ships and barges, Ocean Engineering, 2001. https://doi.org/10.1016/S0029-8018(00)00036-6.

7. Fernandes AC, Oliveira AC. The roll damping assessment via decay model testing (new ideas about an old subject), Journal of Marine Science and Application, 2009. https://doi.org/10.1007/s11804-009-8107-z.

8. Bo Y, Zuo-Chao W, Ming W. Numerical simulation of naval Ship's roll damping based on CFD, Procedia Engineering, 2012. https://doi.org/10.1016/j.proeng.2012.04.241.

9. de Oliveira AC, Carlos Fernandes A. The nonlinear roll damping of a FPSO hull, Journal of Offshore Mechanics and Arctic Engineering, 2014. https://doi.org/10.1115/1.4025870.

10. Begovic E, Day AH, Incecik A, Mancini S, Pizzirusso D. Roll damping assessment of intact and damaged ship by CFD and EFD methods. In Proceedings of the 12th International Conference on the Stability of Ships and Ocean Vehicles, Glasgow, UK, 2015.

11. Hashimoto H, Omura T, Matsuda A, Yoneda S, Stern F, Tahara Y. Several remarks on EFD and CFD for ship roll decay, Ocean engineering, 2019. https://doi.org/10.1016/j.oceaneng.2019.05.064.

12. Song SS, Kim SH, Paik KJ. Determination of linear and nonlinear roll damping coefficients of a ship section using CFD, Brodogradnja, 2019. https://doi.org/10.21278/brod70402.

13. Handschel S, Abdel-Maksoud M. Improvement of the harmonic excited roll motion technique for estimating roll damping, Ship Technology Research, 2014. https://doi.org/10.1179/str.2014.61.3.001.

14. Wassermann S, Feder DF, Abdel-Maksoud M. Estimation of ship roll damping—A comparison of the decay and the harmonic excited roll motion technique for a post panamax container ship, Ocean Engineering, 2016. https://doi.org/10.1016/j.oceaneng.2016.02.009.

15. Kianejad SS, Lee J, Liu Y, Enshaei H. Numerical assessment of roll motion characteristics and damping coefficient of a ship, Journal of Marine Science and Engineering, 2018. https://doi.org/10.3390/jmse6030101.

16. Kianejad SS, Enshaei H, Duffy J, Ansarifard N, Ranmuthugala D. Ship roll damping coefficient prediction using CFD, Journal of Ship Research, 63(02), 2019, 108-122.

17. Wilson RV, Carrica PM, Stern F. Unsteady RANS method for

ship motions with application to roll for a surface combatant, Computers & Fluids, 2006. https://doi.org/10.1016/j.compfluid.2004.12.005.

18. van't Veer R, Fathi F. On the roll damping of an FPSO with riser balcony and bilge keels, International Journal of Maritime Engineering, 2011. https://doi.org/10.5750/ijme.v153ia2.858.

19. Avalos GO, Wanderley JB, Fernandes AC, Oliveira AC. Roll damping decay of a FPSO with bilge keel, Ocean Engineering, 2014. https://doi.org/10.1115/omae2013-10797.

20. Igbadumhe JF, Sallam O, Fürth M, Feng R. Experimental determination of non-linear roll damping of an FPSO pure roll coupled with liquid sloshing in two-row tanks, Journal of Marine Science and Engineering, 2020. https://doi.org/10.3390/jmse8080582.

21. Haddara MR, Bass DW. On the form of roll damping moment for small fishing vessels, Ocean Engineering, 1990. https://doi.org/10.1016/0029-8018(90)90021-w.

22. Chun HH, Chun SH, Kim SY. Roll damping characteristics of a small fishing vessel with a central wing, Ocean Engineering, 2001. https://doi.org/10.1016/s0029-8018(00)00066-4.

23. Ali B, Katayama T, Ikeda Y. Roll damping characteristics of fishing boats with and without drift motion, International Shipbuilding Progress, 2004.

24. Ayob AAM, Yaakob O. Roll mitigation of small fishing boat, Journal of Transport System Engineering, 2015.

25. Hasanudin H, Chen JH, Utama IKAP, Hendratmoko H. An Investigation into the Effect of Bilge Keels to the Roll Motion Response of Fishing Vessel, Applied Mechanics and Materials, 2017. https://doi.org/10.4028/www.scientific.net/amm.862.284.

26. Katayama T, Adachi T, Sawae T, Roll damping estimation for small planing Craft. In 13th International Conference on Stability of Ships and Ocean Vehicles. Kobe, Japan, 2018.

27. Zhang Y, Wang P, Yu P, Hu J. Numerical and experimental study on nonlinear roll damping characteristics of trimaran vessel, Ocean Engineering, 2022. https://doi.org/10.1016/j.oceaneng.2022.110778.

28. Zhou YH, Ma N, Shi X, Zhang C. Direct calculation method of roll damping based on three-dimensional CFD approach, Journal of Hydrodynamics, 2015. https://doi.org/10.1016/s1001-6058(15)60470-x.

29. Hasanudin H, Zubaydi A, Aryawan WD. Roll Dynamic Coefficients Approach of Decay Test using the Generalized Reduced Gradient Method (GRG), Journal of Applied Engineering Science, 2023. https://doi.org/10.5937/jaes0-40421.

30. 30. O'Connor PJ, O'Connor N. Causes and prevention of boating fatalities. Accident Analysis & Prevention, 2005. https://doi.org/10.1016/j.aap.2005.03.011.

31. 31. Davis B, Colbourne B, Molyneux D. Analysis of fishing vessel capsizing causes and links to operator stability training, Safety Science, 2019. https://doi.org/10.1016/j.ssci.2019.05.017.

32. Uğurlu F, Yıldız S, Boran M, Uğurlu Ö, Wang J. Analysis of fishing vessel accidents with Bayesian network and Chi-square methods, Ocean Engineering, 2020. https://doi.org/10.1016/j.oceaneng.2020.106956.

33. Kim N, Kim YJ, Ha Y. Experimental study of the free roll decay test for the evaluation of roll damping coefficients, Journal of the Society of Naval Architects of Korea, 2015. https://doi.org/10.3744/snak.2015.52.6.460.